analytical chemistry

ARTICLE

pubs.acs.org/ac

Electropolymerized Self-Assembled Layer on Gold Nanoparticles: Detection of Inducible Nitric Oxide Synthase in Neuronal Cell Culture

Wei Choon Alvin Koh, Pranjal Chandra, Dong-Min Kim, and Yoon-Bo Shim*

Department of Chemistry and Institute of Innovative BioPhysio Sensor Technology, Pusan National University, Busan 609-735, Korea

ABSTRACT: Novel nanostructures of gold nanoparticle (AuNP) encapsulated-conductive polymer have been developed to study biosensor probe materials and utilized to detect the concentration of inducible nitric oxide synthase (iNOS). A 2,2′:5′,5″-terthiophene-3′-benzoic acid (TTBA) monomer was synthesized and self-assembled on gold nanoparticles (AuNPs). The size effects of the AuNPs and TTBA monomer film thickness on the electrode conductivity were examined. Anti-iNOS antibody was covalently bound on an encapsulated-AuNPs polymer layer with self-assembled TTBA. The immunocomplex formation between iNOS and anti-iNOS was directly observed by cyclic voltammetry (CV) and electrochemical impedance spectroscopy (EIS). This study looked at the applicability of the self-assembled TTBA layer where the results indicated an efficient electrochemical response toward iNOS. The calibration plot of the current response vs. iNOS concentration exhibited a linear relationship in the range of 0.001−0.02 μg/mL. The calibration sensitivity of iNOS was 59.4 ± 0.3 mV/μg mL^{-1}. The detection limit of iNOS was determined to be 0.20 ± 0.04 ng/mL based on five time measurements (95% confidence level, $k = 3$, $n = 5$). Further results show that AuNP-encapsulated conductive polymers are good nanostructured materials as biosensor probes and have a potential application in cell biosensors.

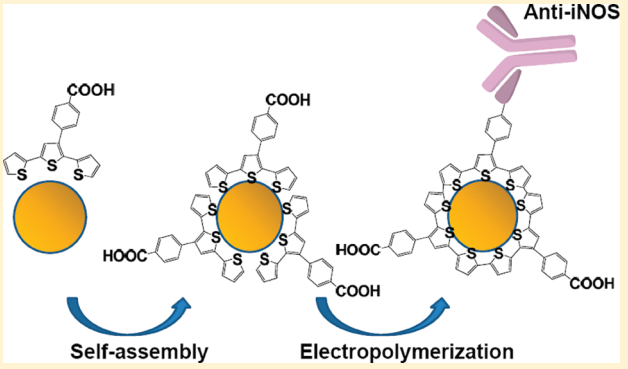

Morphological, structural, and functional complexity is often a defining characteristic of nanomaterials, which involves specific interactions between assembling organic scaffolds.[1−4] These add chemical functionality and thermodynamic stability to the surfaces of relatively simple inorganic nanostructures such as quantum dots, superparamagnetic particles, or nanowires and make it possible to connect them to more complex systems, e.g., biological systems.[5] The presence of a self-assembled layer on the nanoparticles can control the electrostatic nature of the interfaces of individual nanostructures and thus their ability to organize into large assemblies.[6,7] Unraveling the specific interactions between nanoderived templates and organic materials such as conducting polymers not only yields a better understanding of natural hybrid materials but also inspires new methods for developing the potential of biological molecules, superstructures, and organisms as self-assembling agents for biosensor probe fabrication.[8,9]

Gold nanoparticles are readily available, are reasonably inert, are common substrates used for many analytical techniques, and are compatible with cells without evidence of toxicity. The self-assembly of organized organic material on gold nanoparticles (AuNPs) due to the formation of these hybrid nanomaterials on an electrode surface can demonstrate an enormous potential in biosensor fields. In the present work, a novel fabrication method was attempted where the AuNPs were first modified by being encapsulated with self-assembled layers of a precursor monomer so that more reactive carboxylic acid groups were completely facing outward for covalent attachment in forming cross-linked monomer layers. The AuNPs would then be encapsulated in the self-assembled layer after electropolymerization of the precursor monomer into the conducting polymer. This further enhanced the sensor probe performance in terms of higher stability and sensitivity as compared to our previous reports where AuNPs were electrodeposited first onto the probe surface before conducting polymer is attached.[10−12]

As a free-radical gas, NO is synthesized by nitric oxide synthase (NOS) and mediates diverse functions, including vasodilatation, neurotransmission, inhibition of platelet aggregation, immunoresponse, and extracellular matrix production.[13] In the case of inducible nitric oxide synthase (iNOS), macrophages produce NO and tumor necrosis factor-a (TNF-a) in response to various stimuli, such as lipopolysaccharide (LPS). The involvement of NO in nonspecific host defense, macrophage-mediated killing, and the inhibition of the proliferation of microorganisms and tumor cells has been previously demonstrated.[14] To apply the nanostructured iNOS sensor probe in a practical application, we extended our investigation to the detection of iNOS in neuronal cell culture by utilizing the electrochemical iNOS immunosensor. The investigation of the role played by iNOS in NO release is important and it would contribute to our understanding of iNOS function.[15,16] Thus, it is essential to develop a reliable detection

Received: March 15, 2011
Accepted: July 7, 2011
Published: July 07, 2011

ACS Publications © 2011 American Chemical Society

dx.doi.org/10.1021/ac2006558 | *Anal. Chem.* 2011, 83, 6177–6183

method for iNOS. Generally, Western-Blot analysis[17] and fluorescent labeling[18] have been used for detection of iNOS. Other analytical methods, such as electron paramagnetic resonance,[19,20] high-performance liquid chromatography (HPLC),[21,22] and capillary electrophoresis (CE)[23] have also been known to detect iNOS activity indirectly. The enzyme-linked immunosorbent assay (ELISA) is also a standard method for iNOS detection.[24,25] However, these analytical techniques are complicated and time-consuming. Thus, more simple and reliable methods such as electrochemical detection methods are needed for development in that they are less time-consuming, more sensitive, and fast. As of yet, there has been no extensive attempt to obtain more accurate and simple electrochemical methods for the direct determination of iNOS. Hence, a new electrode modification method is needed to enhance the electrochemical biosensor performance. Development of a new strategy showing high sensitivity and stability can be achieved through the fabrication of a probe surface with nanomaterials or nanostructures. To the best of our knowledge, no investigation has been done so far on the direct detection of iNOS using an electrochemical immunosensor.

In the present study, the novel iNOS nanostructured probe was fabricated by the covalent immobilization of a polyclonal antibody onto polymerized 2,2′:5′,5″-terthiophene-3′-benzoic acid (TTBA) self-assembled layer-covered AuNPs with many outward facing functionalized carboxylic acid groups and characterized with X-ray photoelectron spectroscopy (XPS), transmission electron microscopy (TEM), atomic force microscopy (AFM), and electrochemical methods. The immobilization of antibody on the nanostructured probe surface and the antibody−antigen interaction were characterized using cyclic voltammetry (CV) and electrochemical impedance spectroscopy (EIS) techniques. The impedance change and current response due to the specific immuno-interaction observed at the sensor surface was utilized to detect iNOS. Experimental parameters, such as antibody amount, pH, temperature, etc. were optimized. Finally, the proposed immunosensor was successfully applied to neuronal cell samples, and its validity was evaluated.

EXPERIMENTAL SECTION

Materials. A functionalized monomer, 2,2′:5′,5″-terthiophene-3′-benzoic acid (TTBA), was newly synthesized through the Paal-Knorr pyrrole condensation reaction. Human recombinant inducible nitric oxide synthase (iNOS), bovine serum albumin (BSA), 1-ethyl-3-(3-dimethylamino-propyl) carbodiimide (EDC), monoclonal goat antihuman immunoglobulin G (anti-iNOS), 1-ethyl-3-(3-dimethylaminopropyl) carbodiimide (EDC), dichloromethane (CH_2Cl_2) (99.8%, anhydrous, sealed under nitrogen gas), and hydrogen peroxide (30% solution) were purchased from Sigma Aldrich. Tetrabutylammonium perchlorate (TBAP, electrochemical grade) was received from Fluka, purified, and then dried under vacuum at 1.33×10^3 Pa. Disodium hydrogen phosphate, sodium dihydrogen phosphate, sodium chloride, sulfuric acid, and ethanol were purchased from Aldrich Chemical Co. A phosphate buffer saline solution (PBS) was prepared from 0.1 M of disodium hydrogen phosphate, 0.1 M of sodium dihydrogen phosphate, with addition of 0.1% sodium chloride. All other chemicals were of extra pure analytical grade and used without further purification. All aqueous solutions were prepared in doubly distilled water, which was obtained from a Milli-Q water purifying system (18 MΩ cm).

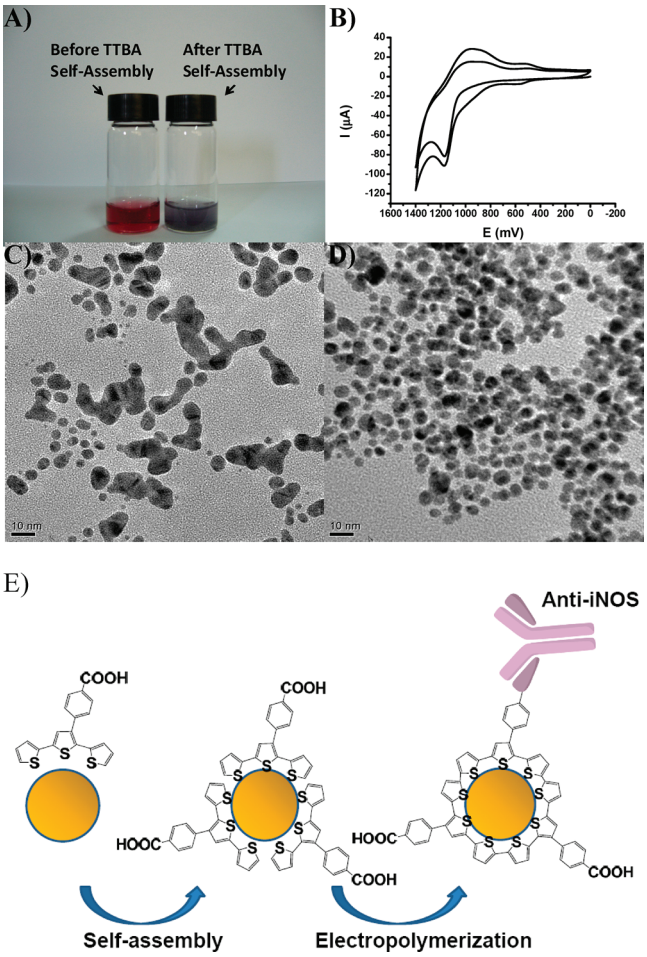

Figure 1. (A) Color changes in AuNP solution before and after TTBA monomer self-assembly. (B) Cyclic voltammogram depicting electropolymerization of AuNPs(TTBA) onto the electrode surface. TEM images of AuNPs (C) without and (D) with a nanolayer of TTBA. (E) Self-assembly scheme of the TTBA monomer layer and electropolymerization of TTBA on AuNPs.

Preparation of the Nanostructured iNOS Sensor Probe. A 0.01% AuNPs solution was prepared from a 0.1 M PBS solution containing 10 mM $HAuCl_4$ and 10 mM trisodium citrate, then adding 0.1 M $NaBH_4$ drop by drop while stirring slowly. A self-assembled TTBA monomer layer onto gold nanoparticles (AuNPs) was formed by mixing 1.0 mM TTBA monomer dissolved in acetonitrile and 0.01% AuNPs (5 nm diameter) at a 1:1 ratio for 12 h at 4 °C. Prior to polymerization, gold probe electrodes were polished with 0.5 μm alumina slurry on a polishing cloth to a mirror finish, followed by rinsing with distilled water. The TTBA-covered AuNP layer was then formed onto the electrode surface through the electropolymerization reaction of TTBA-covered AuNPs in a 0.1 M TBAP/acetonitrile solution by cycling the potential between 0 and 1.6 V two times at the scan rate of 100 mV/s. After that, the electrode was washed with acetonitrile to remove the excess monomer mixture. The schematic presentation of iNOS immunosensor is presented in Figure 1E. As shown, the TTBA-covered AuNP layer coated electrode was immersed for 12 h in a 0.01 M phosphate buffer solution (pH 7.0) containing 20.0 mM of EDC to activate the carboxylic acid groups of the polymer layer. Then, the EDC treated modified electrode was washed with buffer

solution and subsequently incubated for 24 h in 5 mM PBS solution (pH 7.0) containing 0.5 mg/mL anti-iNOS IgG at 4 °C. By this procedure, anti-iNOS IgG was covalently bound through its amine groups to the carboxylic groups on the TTBA-covered AuNP layer forming amide bonds. The next step involved 2 h of pretreatment with the 1% BSA blocking buffer.

Instrument. For the analysis of iNOS, the immunosensor was incubated in iNOS diluted-PBS (0.1 M, pH 7.0) at 25 °C for 15 min and then rinsed with the washing buffer (0.05 M PBS pH 7.0). The iNOS immunosensor, Ag/AgCl (in saturated KCl), and a Pt wire were used as the working, reference, and counter electrodes, respectively. TEM images of TTBA-covered AuNPs were obtained using a Cambridge Stereoscan 240. Electron spectroscopy for chemical analysis (ESCA) experiments were done using a VG Scientific ESCALAB 250 XPS spectrometer with monochromated Al Kα source and charge compensation (Korea Basic Science Institute, Busan). Impedance spectra were recorded with the EG&G PAR 273A potentiostat/galvanostat and a lock-in amplifier (PAR EG&G, model 5210) linked to a personal computer. The frequency was scanned from 100 kHz to 10 or 100 Hz at an open circuit voltage, acquiring 5 points per decade. The amplitude of the sine voltage of 10 mV was used. The measurements were carried out in a buffered medium (0.01 M PBS, pH 7.0) at ambient temperature 25 °C. The impedance Z is expressed in terms of a real (Z_{re}) and an imaginary (Z_{im}) component. Cyclic voltammograms and chronoamperograms were recorded using a potentiostat/galvanostat, Kosentech model KST-P2 (South Korea). Cyclic voltammograms were recorded from −0.6 to 0.6 V versus Ag/AgCl in 0.1 M PBS with pH 7.4. Chronoamperometric experiments were performed by applying the potential of −0.4 V at the iNOS immunosensor. A freshly prepared 4.0 mL aliquot of 0.1 M PBS was added, and the steady state current was monitored with an iNOS immunosensor at optimal pH and temperature. Consecutive injections of varying amounts of iNOS into the electrolytic media and their amperometric responses were monitored. Prior to the cell sample experiments, cell lysing solution was added to the respective neuronal cells in order to lyse the cell membrane and release iNOS into the test solution. In *in vitro* experiments, two electrode configurations were used where the iNOS immunosensor and a micro Ag/AgCl wire acted as the working and reference/counter electrodes, respectively. All immunosensors were calibrated for *in vitro* experiments at 25 ± 1 °C.

Cell Culture Sample. Neuronal C6 and A172 cells (American Type Culture Collection, Manassas, VA) were cultured in Dulbecco's Modified Eagle's Medium (Gibco), supplemented with 15% fetal calf serum (Gibco), 0.1 mM mercaptoethanol (Sigma), 0.1 mM nonessential amino acids (Gibco), 100 U/mL penicillin, and 100 mg/mL streptomycin (Gibco). Briefly, cells were trypsinized and suspended in 10 mL of differentiation medium (Iscove's Modified Dulbecco's Media), 15% FBS, 2.0 mM L-glutamine, 0.1 mM nonessential amino acids, 100 U/mL penicillin, 100 mg/mL streptomycin and cultured in 100 mm nonadhesive Petri dishes to allow cells to aggregate and form embryoid bodies (EBs). Medium was replaced every 2 days. Cells were plated on 0.1% gelatin coated Petri dishes.

RESULTS AND DISCUSSION

Surface Characterization of the Modified Electrode. The formation of the self-assembled TTBA monomer layer on AuNPs (diameter 5 nm) was followed accordingly. In order to facilitate an extremely sensitive surface which can be achieved using nanostructures, the AuNP(TTBA) was first formed by self-assembly of the TTBA monomer on AuNPs and then electropolymerized onto the electrode surface. Figure 1A showed the color changes of the AuNP solution before (dark red at absorption wavelength 700 nm) and after (purple at absorption wavelength 420 nm) formation of the self-assembled TTBA layer on the AuNPs. The nanoparticle comprised conducting polymer layer was obtained through the electropolymerization by cycling the potential between 0 and 1.4 V two times at the scan rate of 100 mV/s. As shown in Figure 1B, an increasing reduction and oxidation peak for AuNP(TTBA) during each potential cycle was obtained at 900 and 1130 mV, respectively. After that, the electrode was washed with acetonitrile to remove the excess TTBA monomer and AuNPs. To obtain TTBA layers onto AuNPs with maximum surface coverage, the effect of the TTBA monomer on the AuNPs ratio during the incubation time at 4 °C was studied. The TEM image in Figure 1C showed the AuNPs without the TTBA monomer layer whereas that of Figure 1D showed a TTBA monomer layer on AuNPs. In Figure 1C, the AuNP particle size was in the range of 5−10 nm and was widely distributed. The thickness of the self-assembled TTBA on the AuNPs was about 4−5 nm. In Figure 1D, the TTBA monomer nanolayer-covered AuNPs formed nanocomposite sphere-shaped clusters of about 10−20 nm in diameter. To obtain AuNP(TTBA) layers with maximum surface coverage, the effect of the scan rate during the electropolymerization experiment was studied. In the present work, a scan rate of 100 mV/s was used in the cyclic voltammetric experiments. The thickness of the AuNP(TTBA) layers after three cycles decreased with increasing scan rate (between 50 and 200 mV/s), indicating the formation of smaller particles at a fast scan rate. The AuNP(TTBA) exhibited high surface area, which gave another advantage to immobilize a large amount of anti-iNOS onto the TTBA-covered AuNP layer. After electropolymerization of TTBA nanocomposite clusters on the electrode surface, a three-dimensional homogeneous compact structure was obtained which possessed good stability and preparation reproducibility. This compact nanostructured TTBA nanocomposite film provided a significant increase in effective active sites for substrates and yielded good electrochemical response. The self-assembled nanolayer on AuNPs was characterized with AFM and ESCA. Figure 2 shows the AFM images and ESCA spectra obtained (part A) before TTBA polymerization, (part B) after TTBA polymerization, and (part C) AuNPs deposited on the polyTTBA surface. The AFM image in Figure 2A showed the (TTBA monomer)AuNPs before polymerization. Upon electropolymerization, the TTBA-functionalized nanoparticles aggregate, forming layers of (polymerized TTBA)AuNPs at a size of about 50 nm as shown in Figure 2B. As observed in Figure 2C using our conventional method of AuNP electrodeposition, the deposited AuNP size was in the range of 10−20 nm. The ESCA C1s spectra for three surfaces were observed at 284.4 eV, while the O1s peak was shown at 531.8 eV. The spectra in parts A, B, and C of Figure 2 also showed peaks at 83.7 and 162.6 eV, corresponding to Au4f and S2p, respectively, where Au4f was absent in the Figure 2B spectrum. In Figure 2C, there was an Au4f peak due to the presence of deposited AuNPs. The presence of the S2p peak in the spectra was due to the presence of the thiophene groups in the TTBA nanostructured layer which was present in all three surfaces. The intensity of the S2p peak was observed to decrease after TTBA polymerization while there was no Au4f peak intensity as shown in Figure 2B.

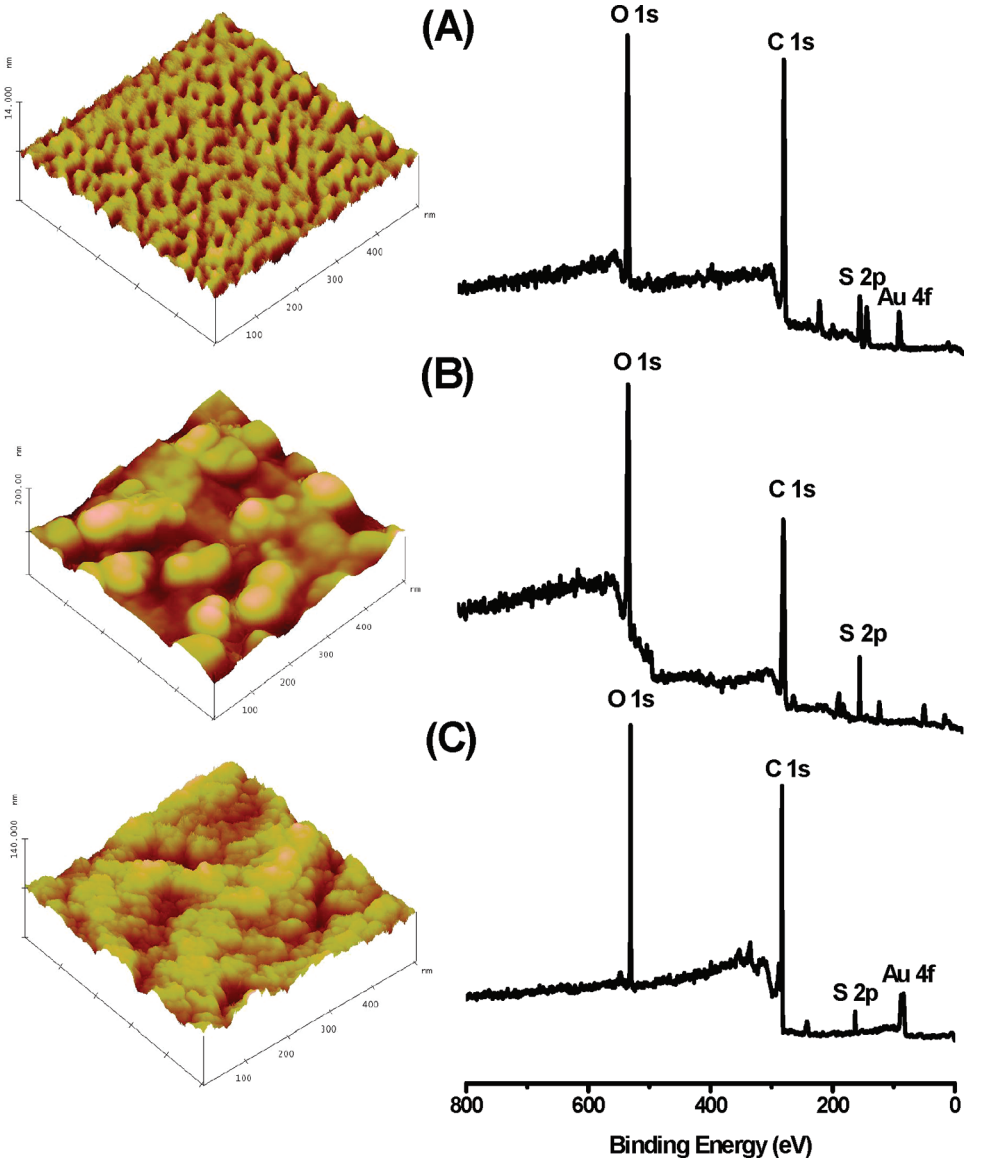

Figure 2. 3D AFM images and ESCA spectra of the electrode surface (A) before TTBA electropolymerization, (B) after TTBA electropolymerization, and (C) with AuNPs electrodeposited on polyTTBA.

This indicates that AuNP surface areas were covered by the TTBA polymer nanolayer.

Impedance spectroscopy was used to further investigate the characteristics of AuNP layers coated with self-assembled TTBA at each modification step. A simple Randle circuit was applied to fit the experimental data for the AuNP(TTBA) layer. Values for the parameters of R_s, R_{ct}, and CPE1, were obtained by fitting the experimental data to the equivalent circuit using Zview2 impedance software. In the equivalent circuit, R_s represents the solution resistance, R_{ct} represents the charge transfer resistance, W represents the Warburg element, and CPE1 is the constant-phase element. Figure 3 shows Nyquist plots obtained for a AuNP(TTBA) modified electrode (circle line), AuNP/TTBA modified electrode (star line), polyTTBA modified electrode (square line), and a bare electrode (triangle line) in a 0.1 M phosphate buffer solution at pH 7.4. The Nyquist plots clearly showed an increase in the charge-transfer resistance due to AuNP(TTBA)

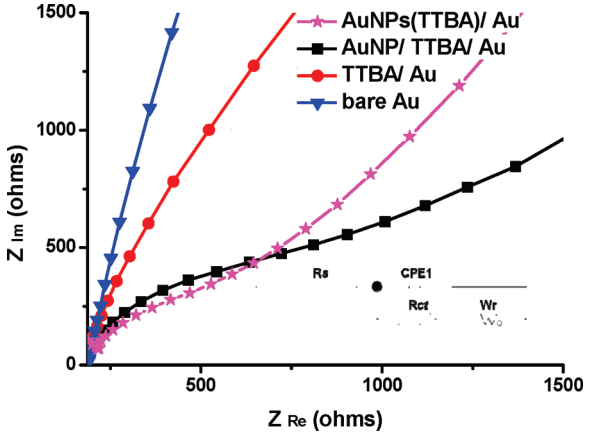

Figure 3. Impedance spectra of different modified layers on the electrode surface before iNOS antibody immobilization.

dx.doi.org/10.1021/ac2006558 |*Anal. Chem.* 2011, 83, 6177–6183

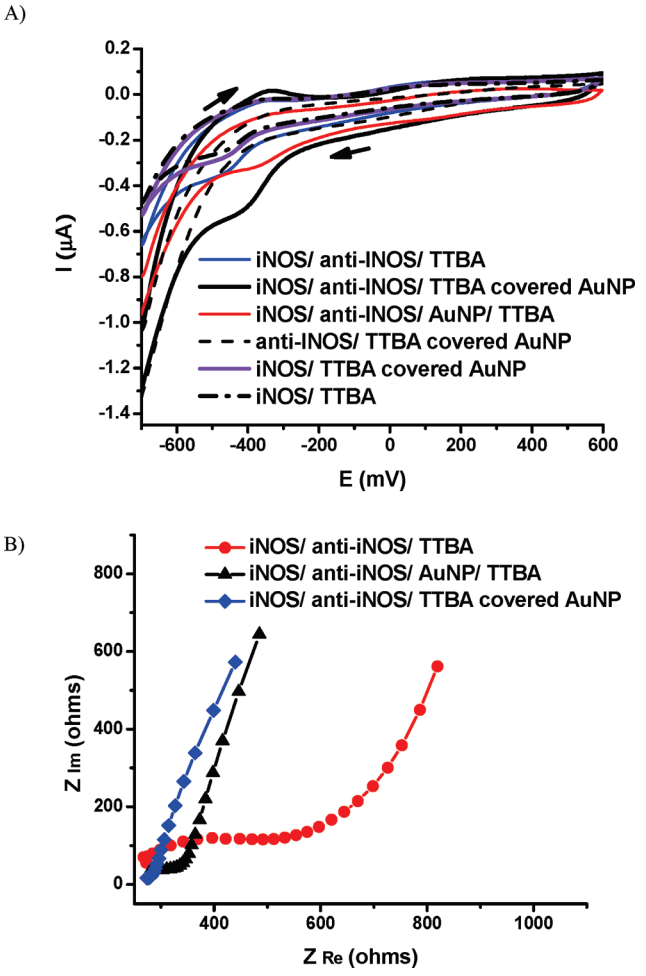

Figure 4. (A) CVs of different modified layers on the electrode surface after iNOS antibody and iNOS immobilization. (B) Impedance spectra of different modified layers on the electrode surface after iNOS antibody and iNOS immobilization.

and AuNP/TTBA. Impedance spectroscopy is an effective method for probing the features of surface-modified electrodes.[26,27] Thus, impedance spectra were obtained for the modified electrodes. The R_{ct} value of a TTBA-only coated electrode was obtained at 1597 Ω cm^2, which was higher than that of the electrodeposited AuNPs-modified surface at 738 Ω cm^2. This showed that AuNPs helped to increase the surface conductivity. A AuNP(TTBA) modified film alters the impedance features at the electrode/electrolyte interface resulting in an even more increase of its electroactive functionality and conductivity. Thus, the R_{ct} value of the AuNP(TTBA) modified electrode was further decreased to 420 Ω cm^2.

Electrochemical Response of iNOS Prior to in Vitro Cell Measurements. To examine the applicability of the polymerized AuNP-TTBA nanostructured sensor probe, we studied the electrochemical activity of iNOS. The response of iNOS was examined *in vitro* as shown in Figure 4A. Cyclic voltammograms (CVs) were recorded for the iNOS/anti-iNOS/AuNP(TTBA) electrodes (black bold line), iNOS/anti-iNOS/AuNP/TTBA modified electrodes (red line), iNOS/anti-iNOS/TTBA modified electrodes (blue line), anti-iNOS/AuNP(TTBA) electrodes (dashed line), iNOS/AuNP(TTBA) electrodes (purple line), and iNOS/TTBA modified electrodes (dashed dotted line) in a 0.1 M phosphate buffer solution at pH 7.4 by cycling the potential between −0.6 and 0.6 V (scan rate 100 mV/s). As seen, there was a pair of redox peaks at −0.35 V (oxidation) and −0.4 V (reduction) in each case whereas there were no redox peaks in the CV recorded with the anti-iNOS/AuNP(TTBA) electrodes. The redox potentials of iNOS on modified electrodes were about −0.2 V versus Ag/AgCl.[28] The redox peak potential was related to the direct electron transfer reaction of iNOS, of which iNOS consists of a reductase domain where electrons are shuttled through bound flavins FAD and FMN, a calmodulin binding region that regulates electron transfer to the heme domain. The iNOS redox peaks at the TTBA-only electrode were observed at more negative potentials of −0.45 V (dashed dotted line). Apparently, the complexation reaction between AuNP(TTBA), anti-iNOS, and iNOS shifted the redox potential in the positive direction on the iNOS-modified electrode. When the CV was recorded for the anti-iNOS/AuNP(TTBA) electrodes in PBS, no redox peak appeared due to the absence of iNOS. This showed that the presence of iNOS increased the redox potential current and shifted the iNOS redox potential slightly toward the negative direction. Moreover, the AuNP(TTBA) layer on the electrodes might have an effect in decreasing the redox potential difference in addition to stabilizing the immobilization of iNOS on the electrode surface. Thus, chronoamperometric experiments were performed at an applied potential of −0.4 V versus Ag/AgCl. The direct current response of iNOS reduction on TTBA modified electrodes was reduced by 15% at −0.4 V. To obtain the rate constant, we first determined the transfer coefficient α by plotting E_p versus log scan rate v where the anodic and cathodic peak potentials are linearly dependent on log v. The graph slopes can be used to estimate the value of α (data not shown). The electron transfer rate constant, k_s, for this process was determined to be 2.2 s^{-1} using the Laviron equation.[29] This quasi-reversible reaction of iNOS provides the basis for the amperometric iNOS detection in neuronal cells.

Impedance spectra were also obtained after iNOS antigen−antibody immunocomplex formation (Figure 4B). The R_{ct} value of iNOS/anti-iNOS/TTBA electrode (357 Ω cm^2) was proven to be higher than that of iNOS/anti-iNOS/AuNP/TTBA (183 Ω cm^2) and iNOS/anti-iNOS/AuNP(TTBA) (69 Ω cm^2) modified electrodes. The iNOS/anti-iNOS/AuNP(TTBA) modified electrode exhibited the highest conductivity as expected for a nanostructured probe surface. The iNOS/anti-iNOS/AuNP(TTBA) modified electrode yields a chemically modified film that alters the impedance features and gives a better detection response of iNOS. This complex formed part of the double-charged layer at the electrode/electrolyte interface resulting in a decrease in the impedance value. After the immobilization and blocking off the free active sites, the anti-iNOS/AuNP(TTBA) modified electrode was incubated for 20 min in a 6.0 μg/mL iNOS solution. The electrode was rinsed with PBS and was used for impedance measurements in a 0.1 M PBS at an open circuit voltage. The interfacial and ionic properties might be changed by the iNOS immunocomplex interaction. The specific iNOS immunocomplex interaction on the AuNP(TTBA) layer resulted in a decrease of impedance. The impedance decrease might have arisen from the change in conductivity or dielectric properties. The maximum difference in impedance values was observed at the frequency of 5.3 × 10^n Hz. The decrease in impedance values was proportional to the concentration of iNOS. This indicates that the impedance decrease was indeed caused by the specific iNOS immunocomplex formation. Hence,

dx.doi.org/10.1021/ac2006558 |*Anal. Chem.* 2011, 83, 6177–6183

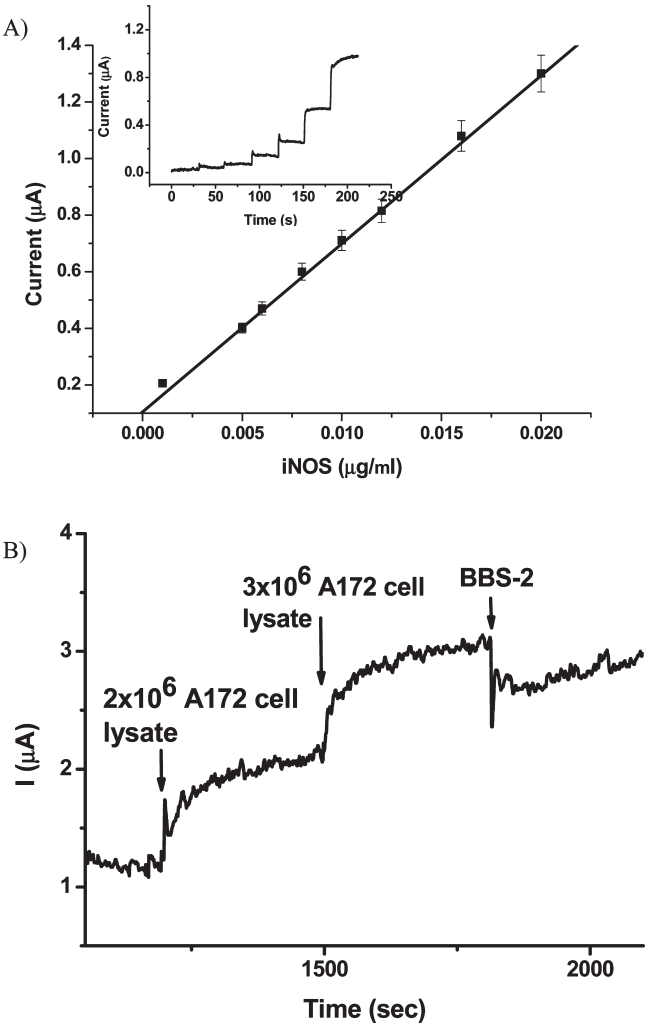

Figure 5. (A) Chronoamperometric response of iNOS immunosensor to varying iNOS concentrations. (Inset) Calibration plot for iNOS immunosensor. (B) Chronoamperometric response of iNOS immunosensor to iNOS released by different cell population numbers of A172 neuronal cells and iNOS inhibitor BBS-2.

the iNOS/anti-iNOS/AuNP(TTBA) modified electrode was used as an iNOS immunosensor for subsequent experiments.

Optimization of Experimental Parameters. To optimize the sensing condition of the iNOS immunosensor, the pH effect of the medium and the applied reduction potential were studied on the electrochemical redox reaction of iNOS with iNOS/anti-iNOS/AuNP(TTBA) modified electrode. The pH effect on analytical sensitivity was studied in the pH range of 4.0−9.0. The response current increased as media pH increased from 4.0 to 7.0 and then showed a decrease above pH 7.5 (data not shown). However, the current response did not decrease significantly between pH 7.0 and 7.5. Since the physiological pH in the brain is considered to be 7.4, the calibration experiments were done at pH 7.4. The effect of the applied reduction potential on the chronoamperometric current response was also studied for the redox reaction of iNOS with the immunosensor. The current response increased as the applied potential went from 0.6 V to more negative potentials up to −0.4 V, where the maximum response was observed. This tied in well with the cyclic voltammetric results in that iNOS showed a reduction peak at the same value −0.4 V. The application of more negative potentials up to −0.9 V showed declining current response (data not shown). Therefore, the iNOS immunosensor was polarized at −0.4 V versus Ag/AgCl in the chronoamperometric experiments.

Selectivity and Long-Term Stability of iNOS Immunosensor. The selectivity of the immunosensor was evaluated in the presence of these reactive species. Before studying the interference effect, the iNOS immunosensor was first incubated in PBS and then a 0.1% BSA solution in PBS in order to saturate the remaining active sites on the anti-iNOS antibody and to block any nonspecific bindings. The presence of a free radical scavenger, 0.1 μM ascorbic acid, removed oxygen interference. Compounds such as 0.2 mM dopamine (DA), 0.1 mM BPA, 0.1 μM L-arginine, 0.1 μM ascorbic acid, 0.1 μM nitrate, and 0.1 μM NO did not significantly interfere in the detection of iNOS (data not shown). The current response value obtained after iNOS binding (0.2 μg/mL) did not significantly change in the presence of another NOS protein isoform (neuronal NOS) even at about 2.5 times higher concentration (0.5 μg/mL). In fact, less than a 3.0% decrease of the iNOS current response was observed in the presence of the above compounds. This means that the presence of such compounds should not interfere significantly with the detection of iNOS, indicating that the immunosensor was highly selective for iNOS. When not in use, the sensors were stored in PBS (pH 7.4) at 4 °C for more than 2 months with a significant loss of 5% original response after the first month followed by a 30% decrease in response after the second month, indicating long-term stability.

Calibration Plot. To calibrate the iNOS immunosensor for *in vitro* cell measurements, the chronoamperometric response of the anti-iNOS/AuNP(TTBA) modified electrode was performed by introducing varying concentrations of iNOS. The presence of the iNOS−anti iNOS complex is to enable the immunosensor to be more specific for the iNOS target molecule in the neuronal cell culture. The experiment is performed after an incubation time of 10 min. This provided for the reaction time between anti-iNOS/AuNP(TTBA) modified electrode and iNOS. Figure 5A showed the calibration plots of the anti-iNOS/AuNP(TTBA) modified electrode during an *in vitro* experiment. Under optimized conditions, the steady-state currents exhibited a linear relationship with the iNOS concentration in the range of 0.001−0.02 μg/mL. Figure 5A (inset) showed the typical current−time plot for the addition of various iNOS concentrations in a 0.1 M PBS solution during *in vitro* experiments. The applied potential was set at −0.4 V for the electroreduction of iNOS by the anti-iNOS/AuNP(TTBA) modified electrode. The response current rose steeply and then arrived at an increased steady value after each addition of iNOS. In total, 95% of steady-state currents were achieved by the anti-iNOS/AuNP(TTBA) modified electrode after about 15 s. The electrode was found to be reusable for eight times and the relative standard deviation was found to be 5.4%, after five experimental runs. The linear dependencies of iNOS concentration gave an equation of i_p (μA) = (0.104 ± 0.002) + (59.4 ± 0.3)[C] (μg/mL), with a correlation coefficient of 0.997. The sensitivity of the iNOS immunosensor was 59.4 ± 0.3 μA/μg mL^{-1}. The detection limit of iNOS was determined to be 0.2 (±0.04) ng/mL by an anti-iNOS/AuNP(TTBA) modified electrode based on five measurements for the standard deviation of the blank noise (95% confidence level, k = 3, n = 5). These results were compared to the standard ELISA method for iNOS detection and were found to be three order magnitudes lower than previously reported for

in vitro iNOS detection.[30] Thus, the highly sensitive iNOS immunosensor was obtained and used in *in vitro* neuronal cell experiments. The probe can be regenerated easily by breakage of the iNOS/anti-iNOS bond and reusing the anti-iNOS immobilized on the modified electrode surface. Glycine-HCl (pH 2.3) buffer containing 1% dimethyl sulfoxide is used as a dissociation buffer.[31] The stability can be maintained for 2 months without any substantial loss in measurement response to iNOS. The immunosensor was found to be reusable for eight times, and the relative standard deviation was found to be 6.2%, after five experimental runs in biological media. In practice, this immunosensor can be employed commercially as selectivity is controlled strictly by the anti-iNOS antibodies.

Cell Culture Sample Analysis. The iNOS immunosensor was first used to probe the concentration change of iNOS in lysed A172 neuronal cells using the chronoamperometry technique. Figure 5B shows the amperometric response of iNOS released by A172 cells at the applied potential of −0.4 V. In the presence of 2.0×10^6 cells, the iNOS immunosensor registered an increased current response of 8.3 ± 0.3 μA, based on five measurements. When a cell buffer solution containing 3.0×10^6 cells was further injected into the well, there was an additional increase of 10.4 ± 0.2 μA in current response, based on five measurements. In addition, an inhibitor BBS-2 (0.1 μM) was added to the cell well and the current response decreased by 2.4 ± 0.2 μA. BBS-2 reacts with the heme group present in iNOS leading to the formation of a BBS-2 and iNOS complex.[32] Thus, it is possible to speculate that the decrease in the current response is not because of either blocking of iNOS production or active site blocking of the iNOS antibody. It is possibly due to complex formation between BBS-2 and iNOS. These results proved that the iNOS immunosensor was effective in monitoring iNOS release by neuronal cells.

CONCLUSIONS

An electropolymerized self-assembled layer on AuNPs can be utilized as an immunosensor to examine the electrochemistry of iNOS in neuronal cell culture. The direct detection of iNOS was achieved by immobilizing a monoclonal anti-iNOS antibody onto the nanostructured sensor probe through covalent bond formation. The nanosurface characterization was studied by both cyclic voltammetry and impedance techniques. The self-assembled layer modified electrode was found to have excellent properties in terms of better conductivity and lower charge transfer resistance. The main advantage of this sensor probe is its simplicity compared to classical immunoassay methods or optical detection based immunosensing systems. The electrochemical immunosensor developed in the present study can directly detect iNOS selectively without a redox probe or enzyme label. The nanostructured sensor probe was successfully applied to neuronal cell samples to detect iNOS, and the results were found to be satisfactory. As such, further developments in the nanostructured iNOS immunosensor system will depend on improvements to interfacial chemistry and these can thus provide a real-time sensor platform for cell toxicity studies.

AUTHOR INFORMATION

Corresponding Author

*Phone: +82 51 510 2244. Fax: +82 51 514 2430. E-mail: ybshim@pusan.ac.kr.

ACKNOWLEDGMENT

This research was supported by the Researcher Program through the National Research Foundation grant funded by the Korea Ministry of Education, Science and Technology (Grant No. 20100029128).

REFERENCES

(1) Rosi, N. L.; Mirkin, C. A. *Chem. Rev.* **2005**, *105*, 1547–1562.
(2) Smith, F. S.; Ceppi, E. D.; Titheradge, M. A. *J. Biol. Chem.* **1997**, *326*, 187–192.
(3) Love, J. C.; Estroff, L. A.; Kriebel, J. K.; Nuzzo, R. G.; Whitesides, G. M. *Chem. Rev.* **2005**, *105*, 1103–1169.
(4) Bain, C. D.; Evall, J.; Whitesides, G. M. *J. Am. Chem. Soc.* **1989**, *111*, 7155–7164.
(5) Templeton, A. C.; Wuelfing, W. P.; Murray, R. W. *Acc. Chem. Res.* **2000**, *33*, 27–36.
(6) Lehn, J. M. *Proc. Natl. Acad. Sci. U.S.A.* **2002**, *99*, 4763–4768.
(7) Naik, R. R.; Stringer, S. J.; Agarwal, G.; Jones, S. E.; Stone, M. O. *Nat. Mater.* **2002**, *1*, 169–172.
(8) Patil, A. J.; Muthusamy, E.; Mann, S. *Angew. Chem., Int. Ed.* **2004**, *43*, 4928–4933.
(9) Shenton, W.; Davis, S. A.; Mann, S. *Adv. Mater.* **1999**, *11*, 449–452.
(10) Rahman, M. A.; Kwon, N.-H.; Won, M.-S.; Choe, E. S.; Shim, Y.-B. *Anal. Chem.* **2005**, *77*, 4854–4860.
(11) Shiddiky, M. J. A.; Shim, Y.-B. *Anal. Chem.* **2007**, *79*, 3724–3733.
(12) Koh, W. C. A.; Rahman, M. A.; Choe, E. S.; Lee, D. K.; Shim, Y.-B. *Biosens. Bioelectron.* **2008**, *23*, 1374–1381.
(13) Xie, O. W.; Cho, H. J.; Calaycay, J.; Mumford, R. A.; Swiderek, K. M. *Science* **1992**, *256*, 225–228.
(14) Nijkamp, F.; Folkerts, G. *Clin. Exp. Allergy* **1997**, *27*, 347–350.
(15) Raman, C. S.; Li, H.; Martasek, P.; Kral, V.; Masters, B. S.; Poulos, T. L. *Cell* **1998**, *95*, 939–950.
(16) Wei, C. C.; Wang, Z. Q.; Wang, Q.; Meade, A. L.; Hemann, C.; Hille, R.; Stuehr, D. J. *J. Biol. Chem.* **2001**, *276*, 315–319.
(17) Zhang, C. S.; Hollocher, T. C.; Kolodziej, A. F.; Orme-Johnson, W. H. *J. Biol. Chem.* **1991**, *266*, 2199–2202.
(18) Griffith, O. W.; Stuehr, D. J. *Annu. Rev. Physiol.* **1995**, *57*, 707–736.
(19) Piao, M.-H.; Yoon, J.-H.; Jeon, G.; Shim, Y.-B. *Sensors* **2003**, *3*, 192–201.
(20) Nam, J. M.; Stoeva, S. I.; Mirkin, C. A. *J. Am. Chem. Soc.* **2004**, *126*, 5932–5933.
(21) Dittmann, K.; Gerhäuser, C.; Klimo, K.; Hamburger, M. *Planta Med.* **2004**, *70*, 909–913.
(22) Zhu, Y.; Nikolic, D.; Van Breemen, R. B.; Silverman, R. B. *J. Am. Chem. Soc.* **2005**, *127*, 858–868.
(23) Chan, G. H. H.; Fiscus, R. R. *Exp. Gerontol.* **2004**, *39*, 387–394.
(24) Mathewsona, A. M.; McPhadenb, A. R.; Wadswortha, R. M. *J. Immunol. Methods.* **2003**, *279*, 163–171.
(25) Noah, N. M.; Alam, S.; Sadik, O. A. *Anal. Biochem.* **2011**, *413*, 157–163.
(26) Bard, A. J.; Faulkner, L. R. *Electrochemical Methods: Fundamentals and Applications*; Wiley: New York, 1980; pp 368−340.
(27) Marletta, M. A. *Cell* **1994**, *78*, 927–930.
(28) Udit, A. K.; Belliston-Bittner, W.; Glazer, E. C.; Nguyen, Y. H.; Gillan, J. M.; Hill, M. G.; Marletta, M. A.; Goodin, D. B.; Gray, H. B. *J. Am. Chem. Soc.* **2005**, *127*, 11212–11213.
(29) Laviron, E. *J. Electroanal. Chem.* **1979**, *101*, 19–28.
(30) Khare, P. D.; Shao-Xi, L.; Kuroki, M.; Hirose, Y.; Arakawa, F.; Nakamura, K. *Cancer Res.* **2001**, *61*, 370–375.
(31) Jiang, X.; Li, D.; Xu, X.; Ying, Y.; Li, Y.; Ye, Z.; Wang, J. *Biosens. Bioelectron.* **2008**, *23*, 1577–1587.
(32) McMillan, K.; Adler, M.; Auld, D. S.; Baldwin, J. J.; Blasko, E.; Browne, L. J.; Chelsky, D.; Davey, D.; Dolle, R. E.; Eagen, K. A.; Erickson, S.; Feldman, R. I.; Glaser, C. B.; Mallari, C.; Morrissey, M. M.; Ohlmeyer, M. H. J.; Pan, G.; Parkinson, J. F.; Phillips, G. B.; Polokoff, M. A.; Sigal, N. H.; Vergona, R.; Whitlow, M.; Young, T. A.; Devlin, J. J. *Proc. Natl. Acad. Sci. U.S.A.* **2000**, *97*, 1506–1511.